Available online at www.sciencedirect.com
SCIENCE DIRECT
Journal of Power Sources 155 (2006) 219–230
JOURNAL OF POWER SOURCES
www.elsevier.com/locate/jpowsour

A two-phase flow and transport model for PEM fuel cells

Lixin You [1], Hongtan Liu *

Department of Mechanical Engineering, College of Engineering, University of Miami, P.O. Box 248294, Coral Gables, FL 33124, USA

Received 11 March 2005; accepted 21 April 2005
Available online 11 July 2005

Abstract

A two-phase flow and multi-component mathematical model with a complete set of governing equations valid in different components of a PEM fuel cell is developed. The model couples the flows, species, electrical potential, and current density distributions in the cathode and anode fluid channels, gas diffusers, catalyst layers and membrane, respectively. The modeling results of typical concentration distributions are presented. The coupling of oxygen concentration, current density, overpotential and potential are shown in the membrane electrode assembly (MEA). The model predicted fuel cell polarization curves for different cathode pressures compared well with our experimental data.
© 2005 Published by Elsevier B.V.

Keywords: Proton exchange membrane (PEM); Fuel cells; Two-phase flow; Mathematical model; Water and thermal management

1. Introduction

A PEM fuel cell sandwich consists of at least an anode, a cathode and a membrane. Hydrogen and oxygen have to be transported to the anode and cathode catalyst layers as reactants by fluid channels and gas diffuser layers (GDLs); while the product water have to be transported from the catalyst layers out to the fluid channels by GDLs. As results of electrochemical reactions at catalyst layers, power and some waste heat are also generated. Two-phase flow and transport play essential roles in the optimum operation of PEM fuel cells. First, the most common polymer membrane used today such as Nafion® has to be hydrated to ensure high proton conductivity. Second, a triple interface (gas, liquid and solid) in the catalyst layers is necessary to ensure high gas reactant fluxes, high proton flux and low electrical and ionic ohmic losses. Finally, GDLs have to have enough open pores to transport gas reactants from fluid channels to catalyst layers while effectively removing excessive liquid water from catalyst layers to fluid channels. If complete flooding occurred in the GDLs or catalyst layers, the maximum gas reactant fluxes will be extremely low due to the low solubilities of hydrogen and oxygen in liquid water. On the other hand, if the catalyst layers and the membrane are dry, the ionic resistance will be too high to produce practical usable currents. Therefore, a balance of gas–liquid two-phase flow is very critical for the operation of PEM fuel cells. At present many of the transport phenomena inside a fuel cell cannot be directly observed or measured; thus making mathematical modeling a critical tool to understand such transport phenomena.

The one-dimensional models by Verbrugge and Hill [1,2], Bernardi and Verbrugge [3,4], and Springer et al. [5] provided good fundamental bases for further PEM fuel cell modeling. Springer et al. [5] presented empirical relations for such parameters as water diffusion coefficient, electro-osmotic drag coefficient, water adsorption isotherms, and membrane conductivities, etc. However, one-dimensional models cannot take into account of the effects of reactants consumption and products generation. Fuller and Newman [6], Nguyen and White [7] developed two-dimensional models. These models assume diffusion is the only mechanism for oxygen transport and did not consider the interaction of the flow with the species field in the channel and gas diffuser. Instead, they prescribed concentration boundary conditions

* Corresponding author. Tel.: +1 305 284 2019; fax: +1 305 284 2580.
E-mail addresses: liyo@chevrontexaco.com (L. You), hliu@miami.edu (H. Liu).
[1] Present address: ChevronTexaco Corporation, USA. Tel: +1 713 954 6027.

0378-7753/$ – see front matter © 2005 Published by Elsevier B.V.
doi:10.1016/j.jpowsour.2005.04.025

Nomenclature

AR_m	membrane resistance ($\Omega\,cm^2$)
A_v	catalyst surface area per unit volume ($cm^2\,cm^{-3}$)
C	mass species fraction
D	diffusion coefficient ($m^2\,s^{-1}$)
E_m	equivalent weight of ionomer ($g\,equiv^{-1}$)
F	Faraday constant (96,493C mol^{-1})
H	Henry constant
i_0	catalyst exchange current density ($A\,cm^{-2}$)
I	current density ($A\,cm^{-2}$)
K	absolute permeability (m^2)
M	molecular weight ($kg\,mol^{-1}$)
n	number of electrons or water transport coefficient in the membrane (number of water molecules carried per proton)
N	molar flux ($mol\,cm^{-2}\,s^{-1}$)
P	pressure (Pa)
R	universal gas constant ($J\,mol^{-1}\,K^{-1}$)
T	temperature (K)
u	velocity vector or the x-direction velocity component ($m\,s^{-1}$)
U	voltage (V)
v	y-direction velocity component ($m\,s^{-1}$)
y	dimension through the MEA (cm)
z_i	charge number of species
[]	activity

Greek letters

α	charge transfer coefficient or net water transfer coefficient in the membrane
δ	thickness of subscripted layer
ε	porosity
γ	multiphase correction factor
ϕ	potential
η	potential difference from equilibrium (overpotential), V
κ	ionic conductivity ($(\Omega\,cm)^{-1}$)
λ	water content in membrane, mol H_2O/equivalent $SO_3{}^{-1}$
μ	fluid dynamic viscosity ($N\,m^{-2}$)
ν	fluid kinematic viscosity ($m^2\,s^{-1}$)
ρ	density ($kg\,cm^{-3}$)
ξ	non-dimensional length
τ	tortuosity

Subscripts and superscripts

0	equilibrium
a	anode
b	bulk properties or back pressure
c	capillary, cathode or catalyst layer
d	dry, porous media or electro-osmotic drag
diff	diffusion
eff	effective property which accounts for porosity, tortuosity and liquid water
f	ionomer film
i	species
g	gas phase
hyd	hydraulic permeation
k	phase k
l	liquid phase
m	ionomer phase
net	net flux
oc	open circuit
solid	solid matrix property
v	vapor or volume
w	wet or water
α	species α

either at the gas channel/gas diffuser interface, or at the catalyst layer/gas diffuser interface. Gurau et al. [8] was the first to use computation fluid dynamics (CFD) in the PEM fuel cells. They presented a unified approach by coupling the flow and transport governing equations in the flow channel and the gas diffuser, but only single-phase and incompressible fluid model was used.

To accurately represent the important transport phenomena in PEM fuel cells, it is well accepted that a two-phase flow model is necessary because both liquid and gaseous phases exist under normal fuel cell operating conditions. Wang [9], Weber and Newman [10] provided good reviews for available two-phase flow models for PEM fuel cells. Of numerous two-phase flow models proposed, rigorous multiphase mixture model is widely used because it can model the interaction of gas and liquid in the porous medium with an acceptable numerical complexity. Wang et al. [11] proposed the concept of threshold current density and modeled the species, velocity field in an air cathode in which both single phase and two-phase flow exist. An independent parallel work by You and Liu [12,13] presented a two-phase flow model for the cathode of PEM fuel cell and the model was used to discuss the detailed two-phase flow species and velocity field as well as the effects of major operating conditions on the liquid saturations. Mazumder and Cole [14] also presented a multiphase mixture model and obtained the liquid water distribution in different components of PEM fuel cell. Berning and Djilali [15] presented a two-phase flow model for GDL and flow channel in both anode and cathode sides; however, the MEA was excluded for simulation. Nam and Kaviany [16] and Pasaogullari and Wang's [17] works further elucidated the effects of fiber structure, porosity, capillary pressures on the liquid water flow in the GDL, which is only one component in a PEM fuel cell sandwich. In all, most of the above two-phase flow model efforts except You and Liu [12,13] focused on the GDLs, they either treated the catalyst layer

as a thin film or just assumed an operating current density. Similarly, they either assumed a net water transfer transport across the polymer membrane or did not consider the water transport at all.

There are several different mechanisms to decide the limiting currents for PEM fuel cells. The maximum reactant species (O_2 or H_2) flux through GDLs with or without liquid water flooding is one of them. As described in You and Liu [18], four different media are essentially present for electrochemical reactions in the catalyst layers. These four media include pores for the gas and for liquid water transfer, membrane material for proton transport, carbon particles for electron transport and catalyst particles to facilitate chemical reactions. The maximum reactant gas fluxes, maximum proton flux across the catalyst layer, enough amounts of effective triple interfaces and the driving forces for the electrochemical reactions (overpotentials) are all possible factors to limit the PEM fuel cell current density. Still, another limiting factor is the maximum liquid water flux through the membrane because it is well known that a minimum water flux is required for a given proton flux across the membrane. If the anode side is dehydrated, protons will be difficult to transport from the anode side to the cathode side, and thus limit the PEM fuel cell current density. A fuel cell model will be incomplete without considering all these components in the coupled manner, neither will it be complete if the catalyst layer is treated as a thin film without considering the two-phase flow in a detailed manner.

Therefore, a complete PEM fuel cell model is necessary since the gas, liquid and proton transport phenomena in the various components of a fuel cell are strongly coupled. The present work is the continuation of previous works on the two-phase flow in the GDL [12,13] and the detailed model on the catalyst layers [18]. In this work, a two-phase multi-component mixture model is used to describe the two-phase flow field in the flow channel and the GDL. The catalyst layer is simulated as a region by a pseudo-homogeneous model, and a homogeneous model based on the dilute solution theory is used for the membrane. All the models are coupled to study the whole sandwich of a PEM fuel cell.

In this comprehensive model, the fluxes of hydrogen and oxygen as well as the water production rate are determined by the local current density. The net water transport flux through the membrane is determined by the electro-osmotic drag, the back diffusion and hydraulic permeation and is used as water flux boundary conditions in the anode and cathode. In turn, the local current density is related to the local oxygen concentration and the overpotential, which is limited by the maximum hydrogen and oxygen flux in the gas diffuser or in the catalyst layer, respectively. In addition, the effects of two-phase flow on the convection and the diffusion on the species transport are simulated.

2. Mathematical model

2.1. The PEM fuel cell principles

A simplified diagram of PEM working principles is shown in Fig. 1. A PEM fuel cell consists of an anode, a membrane and a cathode. Each electrode can be further divided into three regions: the gas channel, the gas diffuser and the catalyst layer. Thus, a PEM fuel cell is divided into seven regions.

Hydrogen from the anode side gas channels transfers through the gas diffuser to the anode catalyst sites where it is oxidized under the action of catalyst according to the following reaction

$$2H_2 \rightarrow 4H^+ + 4e^- \quad (1)$$

The protons (H^+) transport across the polymer membrane to the cathode side. The electrons are transported away from the anode catalyst layer through the GDL, bipolar plate and outer load to the cathode catalyst layer where oxygen is reduced by the following reaction

$$O_2 + 4H^+ + 4e^- \rightarrow 2H_2O \quad (2)$$

To enhance proton transport, the polymer membrane must be in a highly hydrated state. On one hand, water is necessary

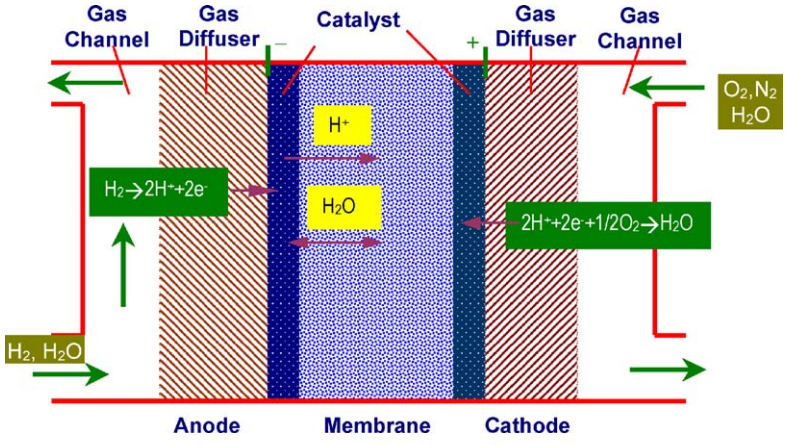

Fig. 1. Schematic illustration of a PEM fuel cell.

to prevent the drying out of the membrane to maintain fuel cell operations. On the other hand, too much water may cause flooding in the pores of the catalyst layer and the gas diffuser, and the reactants (H_2, O_2) are not able to transport to the catalyst sites effectively, which will deteriorate the fuel cell performance.

From the above discussions, the flow, mass transport, current, and potential in the different components in a PEM fuel cell are strongly coupled. For example, the water flux across the membrane depends on the humidification conditions on two sides, the local current density and the membrane properties. In turn, the water flux influences the species field in the cathode and anode sides. Furthermore, the oxygen concentration field affects the local current density; and hence affects the hydrogen, oxygen, and water mass fraction field on both the anode and cathode sides. Liquid water also influences the oxygen transport. Therefore, a complete, two-phase and coupled PEM fuel cell model is essential for the water and thermal management as well as for the improvement of the PEM fuel cell performance.

2.2. Two-phase flow and multi-component model in the cathode

A two-phase multi-component mixture model proposed by Wang and Chen [19] is used for the two-phase flow field of humidified air in the coupled flow channel and the gas diffuser. The governing equations are presented below, and the detailed assumptions and constitutive relations can be found in You and Liu [12].

The governing continuity equation is

$$\varepsilon\frac{\partial\rho}{\partial t}+\nabla\cdot(\rho\mathbf{u})=0 \tag{3}$$

For the two-phase mixture in the gas channel, the Navier–Stokes equation is applicable

$$\frac{\partial(\rho\mathbf{u})}{\partial t}+\nabla\cdot(\rho\mathbf{u}\mathbf{u})=-\nabla P+\nabla\cdot(\nabla\mu\mathbf{u}) \tag{4}$$

For the multiphase mixture flow in the porous gas diffuser, a generalized Darcy law is used [20]

$$\frac{\partial(\rho\mathbf{u})}{\partial t}+\nabla\cdot(\rho\mathbf{u}\mathbf{u})=-\nabla P+\nabla\cdot(\nabla\mu\mathbf{u})-\frac{\mu}{K}(\varepsilon\mathbf{u}) \tag{5}$$

The species conservation equation for the multiphase mixture is [18]

$$\varepsilon\frac{\partial}{\partial t}(\rho C^{\alpha})+\nabla\cdot(\gamma_{\alpha}\rho\mathbf{u}C^{\alpha})=\nabla\cdot(\varepsilon\rho D\nabla C^{\alpha})+\nabla\cdot\left[\varepsilon\sum_k[\rho_k s_k D_k^{\alpha}(\nabla C_k^{\alpha}-\nabla C^{\alpha})]\right]-\nabla\cdot\left[\sum_k C_k^{\alpha}\mathbf{j}_k\right] \tag{6}$$

For the specific system in the PEM fuel cell cathode, the mass fraction equations for oxygen, nitrogen and water can be simplified, respectively as [12],

$$\varepsilon\frac{\partial}{\partial t}(\rho C^{\mathrm{O_2}})+\nabla\cdot(\gamma_{\mathrm{O_2}}\rho\mathbf{u}C^{\mathrm{O_2}})=\nabla\cdot(\varepsilon\rho D_{\mathrm{g}}^{\mathrm{O_2}}\nabla C^{\mathrm{O_2}})-\nabla\cdot\left(\frac{\rho}{\rho_{\mathrm{g}}s_{\mathrm{g}}}C^{\mathrm{O_2}}\mathbf{j}_{\mathrm{g}}\right) \tag{7}$$

$$\varepsilon\frac{\partial}{\partial t}(\rho C^{\mathrm{N_2}})+\nabla\cdot(\gamma_{\mathrm{N_2}}\rho\mathbf{u}C^{\mathrm{N_2}})=\nabla\cdot(\varepsilon\rho D_{\mathrm{g}}^{\mathrm{N_2}}\nabla C^{\mathrm{N_2}})-\nabla\cdot\left(\frac{\rho}{\rho_{\mathrm{g}}s_{\mathrm{g}}}C^{\mathrm{N_2}}\mathbf{j}_{\mathrm{g}}\right) \tag{8}$$

$$\varepsilon\frac{\partial}{\partial t}(\rho C^{\mathrm{H_2O}})+\nabla\cdot(\gamma_{\mathrm{H_2O}}\rho\mathbf{u}C^{\mathrm{H_2O}})=\nabla\cdot(\varepsilon\rho D_{\mathrm{g}}^{\mathrm{H_2O}}\nabla C^{\mathrm{H_2O}})-\nabla\cdot\left[\varepsilon\rho_{\mathrm{l}}D_{\mathrm{g}}^{\mathrm{H_2O}}\nabla s_{\mathrm{l}}\right]-\nabla\cdot\left[\left(\frac{\rho_{\mathrm{v}}^{\mathrm{H_2O}}}{\rho_{\mathrm{g}}}-1\right)\mathbf{j}_{\mathrm{g}}\right] \tag{9}$$

Similar equations can be derived for the anode side.

2.3. Governing equations for electrochemical reaction in the catalyst layer

A pseudo-homogeneous model [18,21,22] is used to simulate the catalyst layer in this work. Four different media are usually present for the proper function of catalyst layer: a diffusion path for reactants and products transfer, an ionic conducting medium for proton transfer, an electrical conduction medium for electrons, and a catalytic surface for electrochemical reaction to take place.

We consider the composite catalyst layer as a homogenous medium. From the oxygen mass–current balance [18], we get

$$\frac{\mathrm{d}I_y}{\mathrm{d}y}=-4F\frac{\mathrm{d}N}{\mathrm{d}y} \tag{10}$$

The kinetic expression for the oxygen reduction rate can be described by Butler–Volmer equation if assuming reduction current is positive

$$\frac{\mathrm{d}I_y}{\mathrm{d}y}=-A_{\mathrm{v}}i_0^{+}\left\{\exp\left(\frac{\alpha_{\mathrm{a}}F\eta}{RT}\right)-\exp\left(\frac{-\alpha_{\mathrm{c}}F\eta}{RT}\right)\right\} \tag{11}$$

where $i_0^{+}=i_0^{\mathrm{ref}+}(C_{\mathrm{O_2}}^{\mathrm{f}}/C_{\mathrm{O_2}}^{\mathrm{ref}})$ and $i_{\mathrm{o}}^{\mathrm{ref}+}$ is reference exchange current density.

When water flow velocities in the catalyst layer are neglected, from Ohms law we have,

$$\frac{\mathrm{d}\phi}{\mathrm{d}y}=\frac{I_y}{\kappa_{\mathrm{eff}}} \tag{12}$$

Since

$$\eta=E-E_{\mathrm{eq}}=\phi_{\mathrm{solid}}-\phi \tag{13}$$

where η is negative in the cathode catalyst layer. The carbon matrix phase can be regarded as equal-potential; changes in

overpotential can be expressed as

$$\frac{\mathrm{d}(-\eta)}{\mathrm{d}y} = \frac{I_y}{\kappa_{\mathrm{eff}}} \tag{14}$$

According to Fick's law, the oxygen flux is related to the oxygen concentration by

$$N_{\mathrm{O_2}} = -D_{\mathrm{O_2}}^{\mathrm{eff}} \frac{\mathrm{d}C_{\mathrm{O_2}}^{\mathrm{f}}}{\mathrm{d}y} \tag{15}$$

where $C_{\mathrm{O_2}}^{\mathrm{f}}$ is the molar concentration of oxygen in the ionomer, which is related to the molar concentration of oxygen in the gas phase $C_{\mathrm{O_2}}^{\mathrm{g}}$ by the Henry's law

$$C_{\mathrm{O_2}}^{\mathrm{f}} = HC_{\mathrm{O_2}}^{\mathrm{g}} \tag{16}$$

where H is Henry constant.

$D_{\mathrm{O_2}}^{\mathrm{eff}}$ in Eq. (15) is the effective oxygen diffusion coefficient given by,

$$D_{\mathrm{O_2}}^{\mathrm{eff}} = \frac{\varepsilon^{1.5} D_{\mathrm{O_2}}}{\tau} \tag{17}$$

Four unknowns, I_y, η, $N_{\mathrm{O_2}}$, $C_{\mathrm{O_2}}$ are described by Eqs. (10), (11), (14) and (15). Boundary conditions for the four equations are,

At $\xi = 0$ (the gas diffuser/catalyst layer interface)

$$I_y = 0 \tag{18}$$

$$N_{\mathrm{O_2}} = \frac{I_\delta}{4F} \tag{19}$$

$$C_{\mathrm{O_2}} = C_{\mathrm{O_2}}^{\xi=0} \tag{20}$$

At $\xi = 1$ (the catalyst layer/membrane interface)

$$\frac{\mathrm{d}(-\eta)}{\mathrm{d}y} = \frac{I_\delta}{\kappa_\delta^{\mathrm{eff}}} \tag{21}$$

2.4. Mathematical model for the membrane

A generalized expression for species transport in the moderately dilute solution is [23]

$$N_{\mathrm{i}} = \frac{-z_{\mathrm{i}} D_{\mathrm{i}} F C_{\mathrm{i}} \nabla\phi}{RT} - D_{\mathrm{i}} \nabla C_{\mathrm{i}} - D_{\mathrm{i}} C_{\mathrm{i}} \nabla \ln a_{\mathrm{i},n} + C_{\mathrm{i}} v \tag{22}$$

The first term on the RHS is zero since water is not charged, the second term is the diffusion term, the third term takes into account non-ideal solution behavior, which is neglected here, and the final term represents the net transport due to bulk flow.

The net water flux is the sum of above water transport flux and the flow induced by the electro-osmotic drag

$$N_{\mathrm{w}}^{\mathrm{net}} = \frac{n_{\mathrm{d}} I}{F} + N_{\mathrm{w}}^{\mathrm{diff}} + C_{\mathrm{w}} v = \frac{n_{\mathrm{d}} I}{F} - D_{\mathrm{w}} \frac{\mathrm{d}C_{\mathrm{w}}}{\mathrm{d}y} - C_{\mathrm{w}} \frac{K_{\mathrm{m}}}{\mu} \frac{\mathrm{d}P_{\mathrm{w}}}{\mathrm{d}y} \tag{23}$$

The net water flux can be expressed as net water transport coefficient [5,24,25]

$$\alpha = \frac{F}{I} N_{\mathrm{w}}^{\mathrm{net}} = n_{\mathrm{d}} - n_{\mathrm{diff}} - n_{\mathrm{hyd}} \tag{24}$$

where

$$n_{\mathrm{d}} = 2.5 \frac{\lambda}{22} \tag{25}$$

$$n_{\mathrm{diff}} = D_{\mathrm{w}} \frac{F}{I} \frac{\mathrm{d}C_{\mathrm{w}}}{\mathrm{d}y} \tag{26}$$

$$n_{\mathrm{hyd}} = C_{\mathrm{w}} \frac{K_{\mathrm{m}}}{\mu} \frac{F}{I} \frac{\mathrm{d}P_{\mathrm{w}}}{\mathrm{d}y} \tag{27}$$

The number of water molecules per sulfonate group, λ, is usually used to express the water content in the membrane. It is related to the water molar concentration by [21]

$$C_{\mathrm{w}}^{\mathrm{m,w}} = \frac{a_{\mathrm{d}} \lambda}{c_{\mathrm{d}} \lambda + 1} \tag{28}$$

where

$$a_{\mathrm{d}} = \frac{\rho_{\mathrm{m,d}}}{E_{\mathrm{m}}} \tag{29}$$

$$c_{\mathrm{d}} = \frac{\rho_{\mathrm{m,d}} M_{\mathrm{w}}}{\rho_{\mathrm{w}} E_{\mathrm{m}}} \tag{30}$$

The diffusive water transport can be simplified as

$$N_{\mathrm{w}}^{\mathrm{diff}} = -D_{\mathrm{w}} \nabla C_{\mathrm{w}} \tag{31}$$

For one-dimensional case

$$N_{\mathrm{w}}^{\mathrm{diff}} = -D_{\mathrm{w}} \frac{\mathrm{d}C_{\mathrm{w}}}{\mathrm{d}y_{\mathrm{m,w}}} \tag{32}$$

where $y_{\mathrm{m,w}}$ is the wet membrane thickness considering the change of membrane dimensions with the water activity

$$y_{\mathrm{w}} = (c_{\mathrm{d}} \lambda + 1)^{1/3} y_{\mathrm{d}} \tag{33}$$

Since

$$\frac{\mathrm{d}C_{\mathrm{w}}^{\mathrm{m,w}}}{\mathrm{d}y_{\mathrm{m,w}}} = \left(\frac{\mathrm{d}C_{\mathrm{w}}^{\mathrm{m,w}}}{\mathrm{d}\lambda}\right)\left(\frac{\mathrm{d}\lambda}{\mathrm{d}y_{\mathrm{m,w}}}\right) \tag{34}$$

solving for the gradient in λ yields

$$\frac{\mathrm{d}\lambda}{\mathrm{d}y_{\mathrm{m,w}}} = -\frac{N_{\mathrm{w}}^{\mathrm{diff}}}{D_{\mathrm{w}}^{\mathrm{m,w}}} \frac{1}{(\mathrm{d}C_{\mathrm{w}}/\mathrm{d}\lambda)} \tag{35}$$

After rearranging and substituting Eq. (23) into Eq. (35)

$$\frac{\mathrm{d}\lambda}{\mathrm{d}y_{\mathrm{m,w}}} = -\frac{N_{\mathrm{w}}^{\mathrm{net}} - (I_{\delta_{\mathrm{c}}} n_{\mathrm{d}}/F) - C_{\mathrm{w}} v}{D_{\mathrm{w}}(\mathrm{d}C_{\mathrm{w}}/\mathrm{d}\lambda)} \tag{36}$$

The membrane resistance $\mathrm{AR_m}$ is calculated by integrating over the membrane thickness by the following equation

$$\mathrm{AR_m} = \int_0^{\delta_{\mathrm{m}}} \frac{\mathrm{d}y_{\mathrm{w}}}{\kappa(\lambda)} = \int_0^{\delta_{\mathrm{m}}} \frac{(c_{\mathrm{d}}\lambda + 1)^{1/3}\,\mathrm{d}y_{\mathrm{d}}}{\kappa(\lambda)} \tag{37}$$

2.5. Fuel cell performance

Cell voltage is calculated as

$$U = U_{oc} - I\mathrm{AR}_m - |\eta_c|_{\xi=1} \tag{38}$$

where $|\eta_c|_{\xi=1}$ is the activation overpotential at the membrane/catalyst layer interface, AR_m can be predicted from Eq. (37). The activation and concentration overpotentials at the anode are much smaller than those at the cathode, and thus are neglected here. The open circuit voltage can be determined from Nernst equation [26].

$$U_{oc} = 1.23 - 0.9 \times 10^{-3}(T - 298) + \frac{RT}{4F} \ln \frac{[H_2]^2[O_2]}{[H_2O]} \tag{39}$$

2.6. Boundary conditions and numerical algorithm

On the anode side, hydrogen and water fluxes at the gas diffuser/catalyst layer interface are related to local current density, respectively, as

$$N_{H_2} = \frac{M_{H_2}}{2F} I \tag{40}$$

$$N_{w,a} = \alpha \frac{M_w}{F} I \tag{41}$$

On the cathode side, oxygen and water fluxes are, respectively,

$$N_{O_2} = \frac{M_{O_2}}{4F} I \tag{42}$$

$$N_{w,c} = -\frac{M_w(1 + 2\alpha)}{2F} I \tag{43}$$

The mixture vertical velocities at the gas diffuser/catalyst layer interface for the anode side and the cathode side are, respectively,

$$\varepsilon v_a \Big|_{y=d_1+d_2} = \frac{N_{H_2} + N_{w,a}}{\rho} \Big|_{y=d_1+d_2} \tag{44}$$

$$\varepsilon v_c \Big|_{y=d_1+d_2} = \frac{N_{O_2} + N_{w,c}}{\rho} \Big|_{y=d_1+d_2} \tag{45}$$

From the Darcy's law, the pressure gradient at the gas diffuser/catalyst layer interface is

$$\frac{dP}{dy} = -\frac{\mu}{K} v \tag{46}$$

If natural convection is neglected, the species concentration gradient can be obtained from,

$$-D\frac{\partial(\rho C_\alpha)}{\partial y} = N_\alpha - \gamma_c \rho \varepsilon v C_\alpha \tag{47}$$

At the inlets, the velocities are given. The standard exit boundary and no-slip boundary conditions are used at the channel right outlet and lower boundary, respectively. For the species field, the inlet species concentrations are known, and the species gradient is zero at the lower boundary and the right exit boundary.

The governing equations in the cathode side, anode side, catalyst layer and membrane are solved simultaneously to ensure the coupling of the flow, species, electrical potential and current density distribution in the cathode and anode fluid channels, gas diffusers, catalyst layers and the membrane.

The numerical procedure is given in the following. First, the overpotential at the catalyst layer/membrane interface is assumed; the governing equations in the catalyst layer are solved by the relaxation method to find the local current density and the oxygen mass flux. From the local current density, the net water flux across the membrane is determined. Then, the oxygen and water fluxes are substituted back into the cathode side governing equations as boundary conditions; meanwhile, the hydrogen and water fluxes are substituted back into the anode side governing equations. Thus, the flow and species field in the cathode side are coupled with the flow and species field in the anode side, the electrochemical reaction in the catalyst layer, and the water transport in the membrane. Therefore, the flow and species are coupled with the current and potential in the catalyst layer and in the membrane. All the coupled equations are solved iteratively. Once the converged solutions are obtained, the cell average current density is obtained as an arithmetic average of all local current densities along the flow direction. By changing the input overpotential incrementally, different current densities and the polarization curve is obtained.

3. Results and discussions

By solving the flow continuity, momentum, and species conservation equations in the cathode and in the anode, respectively, along with the governing equations in the

Table 1
The base case parameters in the model

Channel length (cm)	7.0
Channel width (cm)	0.1
Gas diffuser thickness (cm)	0.03
Catalyst layer thickness (cm)	1.29×10^{-3}
Membrane thickness (cm)	1.0×10^{-2}
Gas diffuser porosity	0.4
Catalyst layer porosity	0.25
Air velocity ($m\,s^{-1}$)	0.35
Hydrogen velocity ($m\,s^{-1}$)	0.6
Air humidification temperature (°C)	60
Hydrogen humidification temperature (°C)	60
Air pressure (Pa)	3.039×10^5
Hydrogen pressure (Pa)	1.013×10^5
Fuel cell temperature (°C)	80
Catalyst surface area ($cm^2\,cm^{-3}$)	1.4×10^5
Exchange current density ($A\,cm^{-2}$)	4.84×10^{-8}
Cathodic transfer coefficient	0.52
Anodic transfer coefficient	0.54
Dry membrane density ($kg\,m^{-3}$)	2.16
Ionomer equivalent weight	1100

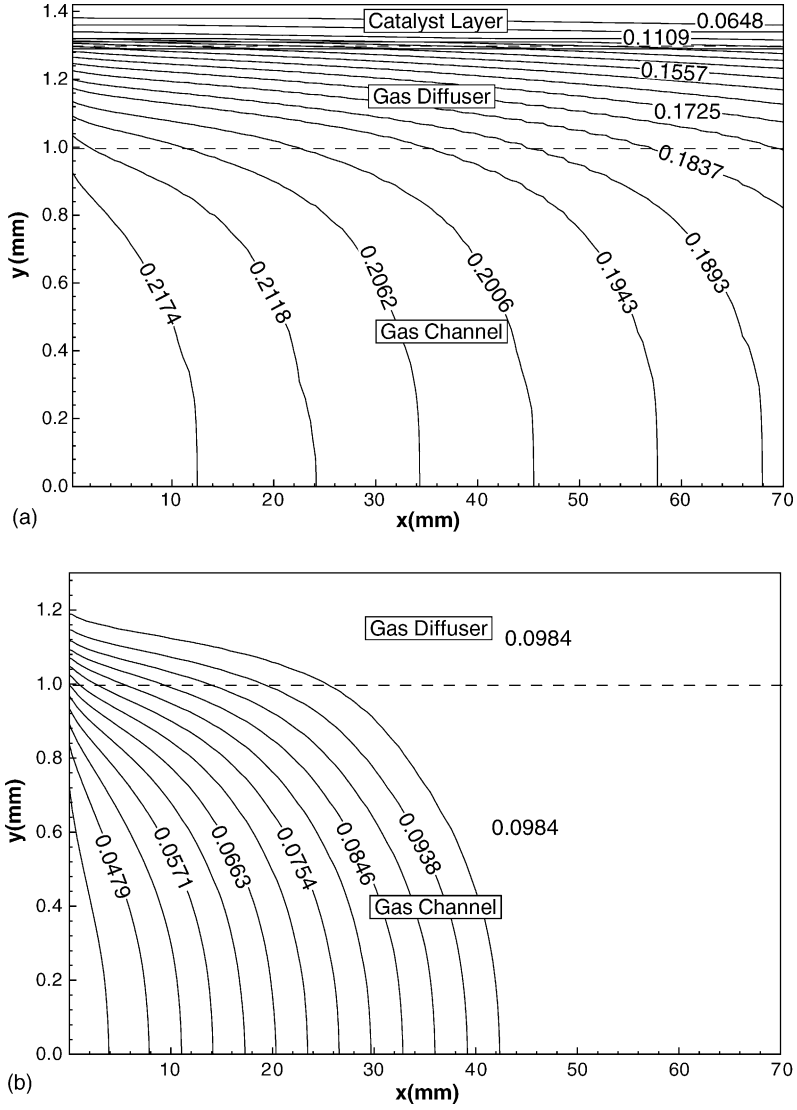

Fig. 2. Oxygen and water vapor mass fraction in the cathode side for the base case with $I_{avg} = 1.09\ A\ cm^{-2}$ (a) oxygen; (b) water vapor.

catalyst layer and in the membrane, the performances of PEM fuel cell can be predicted. Table 1 lists the main geometric and operating parameters for the base case.

A systematic numerical test has been conducted to ensure the simulation results are grid-independent.

3.1. Species concentration in the cathode, anode and membrane

Fig. 2 shows the cathode-side oxygen and water vapor mass fraction on the cathode side at an overall fuel cell current density of $1.07\ A\ cm^{-2}$. The thickness of the catalyst layer in Fig. 2a is enlarged 10 times for a clearer illustration. The oxygen fraction decreases along the flow direction due to the oxygen consumption in the catalyst layer. Considering the enlarged scale for the catalyst layer, it is obvious that the oxygen mass fraction gradient in the catalyst layer is much higher than those in the gas diffuser and gas channel. Fig. 2b shows the water vapor mass fraction in the "gas phase" mixture. Because the air humidification temperature is less than the fuel cell operation temperature, the inlet air is unsaturated. The vapor mass fraction increases along the channel due to the evaporation of liquid water from the catalyst layer. When the air reaches a saturated state, liquid water cannot further evaporate and remains in the liquid state. The line dividing the saturated and unsaturated region is referred to "saturation line" hereafter. Fig. 2b shows that the water vapor fraction increases at the inlet of the channel and becomes constant after the saturation line.

A detailed discussion on the influences of fuel cell operating temperature, cathode and anode humidification temperatures on the two-phase flow can be found in You and Liu [12].

Fig. 3 shows the corresponding water concentration contour in the membrane, where $\xi = 0$ is at the anode

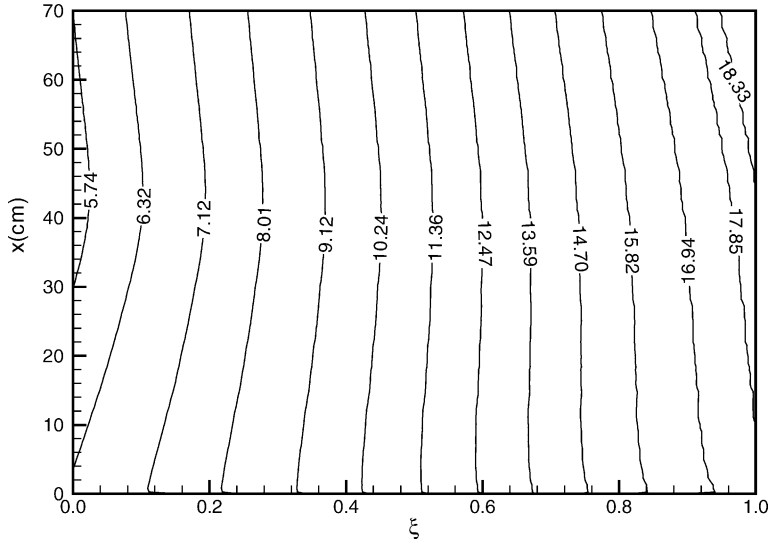

Fig. 3. Water concentration contour in the membrane for the base case with $I_{avg} = 1.09\ A\ cm^{-2}$.

catalyst layer/membrane interface and $\xi = 1$ is at the membrane/cathode catalyst layer interface. The water concentration at the two boundary sides of the membrane are determined by the water activities in the anode side and in the cathode side, respectively [5]. The membrane uptakes water from the humidified gases at two major surfaces. The water profile across the membrane depends on the electro-osmotic drag coefficient, back diffusion and hydraulic permeation. Corresponding to the water activities in the anode and cathode sides, the water concentration decreases along the anode catalyst layer/membrane interface ($\xi = 0$) and increases along the cathode catalyst layer/membrane interface. The total protonic conductance of the membrane depends on the water concentration profiles.

3.2. Coupling of species concentrations current and potential across the MEA

Fig. 4 shows the variation of oxygen concentration across the MEA at $x = 2.5$ mm for four different average fuel cell current densities. The thickness of catalyst layer in this figure is also enlarged 10 times. The oxygen mass fraction has the highest gradient in the catalyst layer due to the highest oxygen transport resistance and oxygen consumption. The oxygen mass fraction gradient in the gas diffuser is also higher than that in the fluid channel, owing to higher transport resistance and much lower convection effect in the porous gas diffuser. When the current density is low, oxygen flux is low, and so is the gradient of oxygen concentration. With the increase of

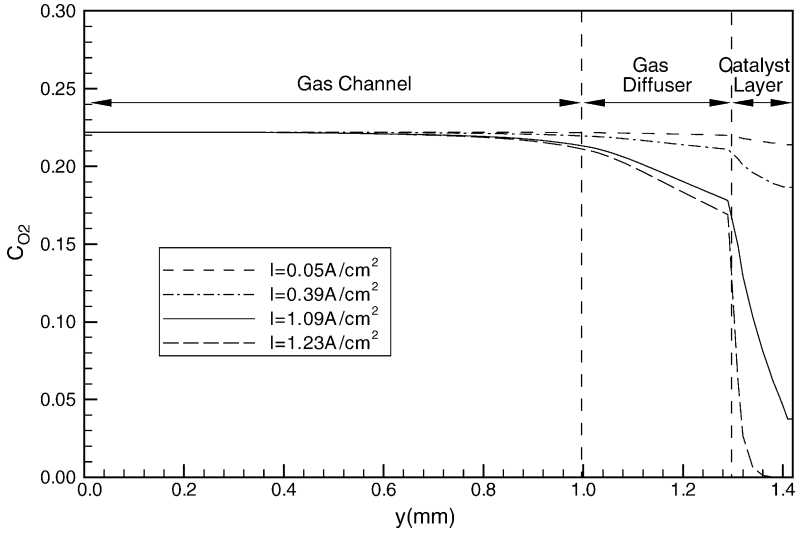

Fig. 4. The variation of oxygen mass fraction across the MEA for the base case with four different current densities.

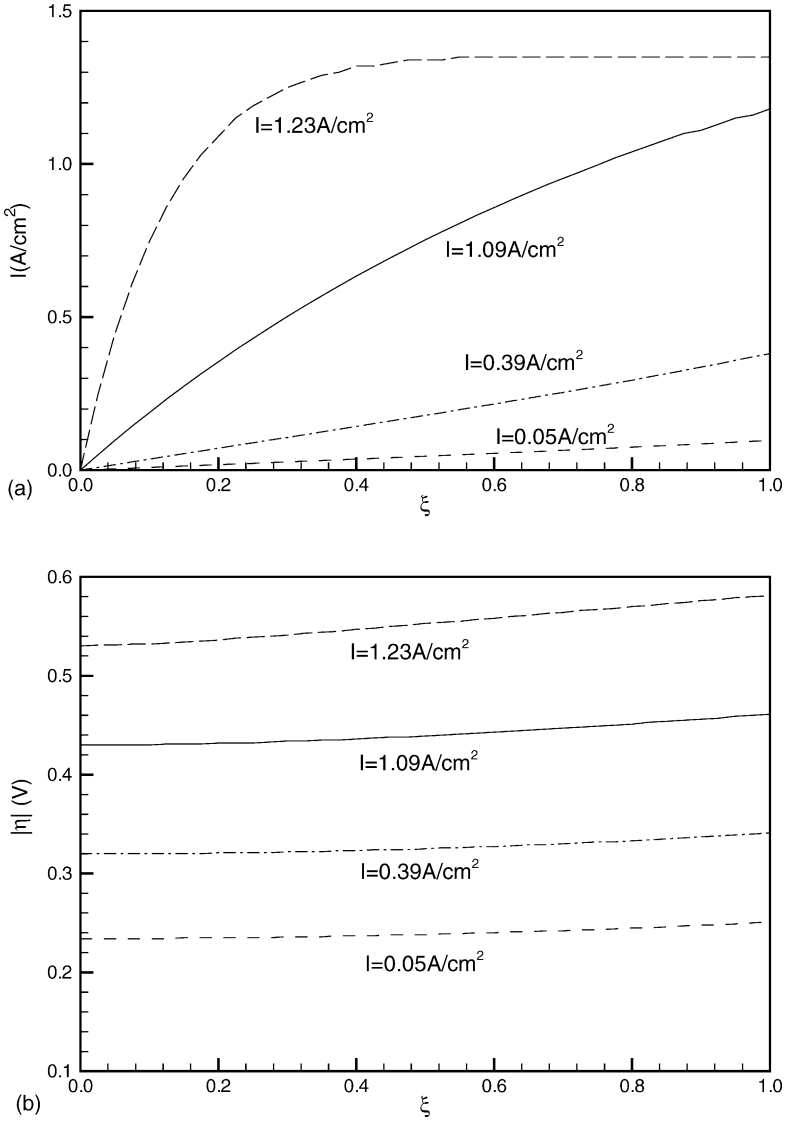

Fig. 5. The variation of current density and overpotential across the cathode catalyst layer for the base case with four different current densities.

current density, more oxygen is consumed and the oxygen concentration in the catalyst layer decreases. With further increase of current density (e.g. $I = 1.23\ \mathrm{A\,cm^{-2}}$), most oxygen is consumed in a region of the catalyst layer close to the gas diffuser, which can be called the "active region". The remaining region where no oxygen is present can be called the "inactive region". Because of oxygen mass-transport limitation, the inactive region does not contribute to the production of current. At a given current density, increasing oxygen concentration and lowering oxygen reduction overpotential are favorable to minimize the inactive region. This can be realized by decreasing liquid volume fraction and gas diffusion paths as well as increasing gas diffuser porosity, stoic ratio and air pressure.

Fig. 5 shows the variation of proton current density and overpotential, respectively, across the catalyst layer corresponding to the oxygen distribution in Fig. 4. The proton current in Fig. 5a is zero at the gas diffuser/catalyst layer interface ($\xi = 0$). It increases across the catalyst layer due to oxygen reduction and reaches the maximum at the catalyst layer/membrane interface ($\xi = 1$). When the local current density is small, the current is generated almost homogeneously across the catalyst layer. With the increase of current density, the current generation rate becomes non-uniform. Most current is generated in the "active region".

Fig. 5b shows the corresponding variation of overpotential across the catalyst layer. The magnitude of overpotential corresponds to the current density. For the same oxygen concentration, if the overpotential is low, the current density is also low and vice versa. From the definition, overpotential is the potential difference between the electrolyte phase and the solid phase. The electrolyte phase potential decreases from the membrane interface ($\xi = 1$) to the gas diffuser interface ($\xi = 0$) due to the Ohmic loss of proton transfer through the

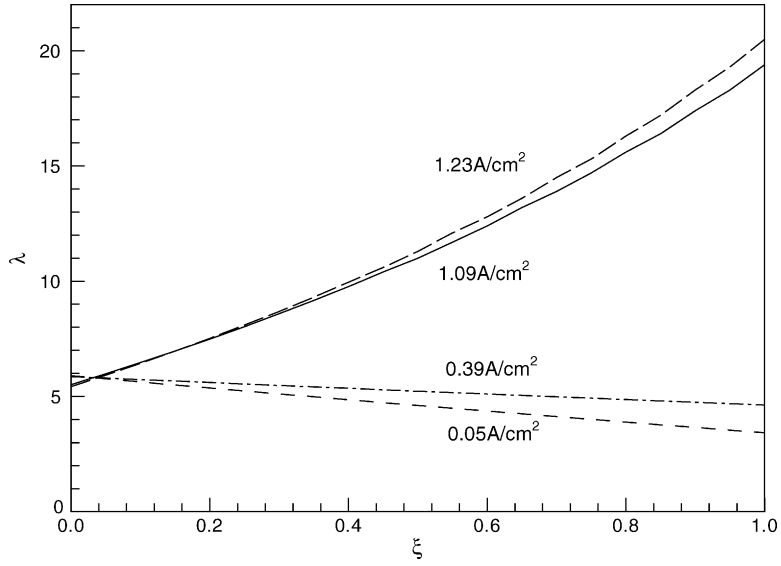

Fig. 6. The water profile in the membrane for different current densities for the base case with four different current densities.

membrane material in the catalyst layer. Because of good electrical conductivity, the potential gradient in the solid carbon matrix can be neglected. Thus, the overpotential has the same tendency as the electrolyte phase potential. The overpotential has the highest absolute value at the catalyst layer/membrane interface and the lowest absolute value at the catalyst layer/gas diffuser interface. The gradient of overpotential is proportional to the proton current if the membrane proton conductivity is constant. Therefore, overpotential difference for high current density is higher than that for low current density.

Fig. 6 shows the water profiles at $x = 2.5$ mm under four different current densities. Here $\xi = 0$ and 1 have the same designations as in Fig. 3. At low current densities, no liquid water is present at the beginning of cathode side, so the water activity in the cathode side is lower than that in the anode side. Therefore, water diffusion has the same direction as the electro-osmotic flux. At higher current densities, more water is produced at cathode and liquid water is present. Thus, the water activity in the cathode side is higher than that in the anode side. As a result, the water diffusion has the opposite direction as the electro-osmotic flux. Because the net water flux is higher at higher current densities, more water is dragged through the membrane from the anode side. Therefore, the water activities in the anode side at higher current densities are lower than those at lower current densities. In contrast, the water activities in the cathode side at higher current densities are higher than those at lower current densities.

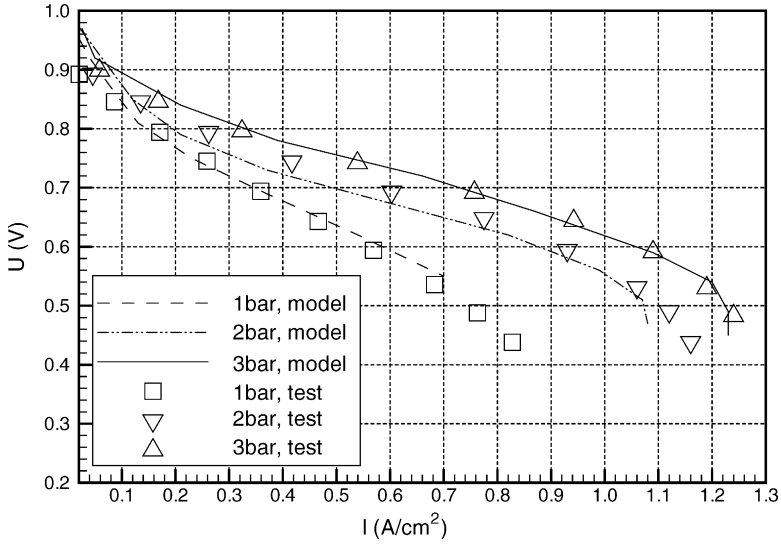

Fig. 7. The comparison of model results with the experimental data for different cathode back pressures at 1, 2 and 3 bar, respectively. Air side: $T_{hyd} = 60\,^{\circ}C$, $u_{in} = 0.35\,m\,s^{-1}$; hydrogen side: $P_b = 1$ bar, $T_{hyd} = 60\,^{\circ}C$, $u_{in} = 0.6\,m\,s^{-1}$; fuel cell operating temperature $T_{cell} = 80\,^{\circ}C$.

3.3. Comparison with experimental data

Fig. 7 shows a group of polarization curves under different cathode pressures from the model compared with experimental data [27]. The fuel cell operating temperature is 80 °C, the humidification temperature is 60 °C for both the cathode and anode, the pressure at the anode is 1 atm, the cathode inlet velocity is 0.6 m s^{-1}, and cathode pressures are at 1, 2, and 3 atm, respectively [27]. It is shown that the modeling results agree with the experimental data reasonably well. With the increase of the cathode pressure, both the oxygen molar concentration and exchange current density increase, which results in the increase of the current generation rates at a given overpotential. Thus, the fuel cell output voltage increases.

4. Conclusions

A two-dimensional, two-phase flow mathematical model with a complete set of governing equations for all the components of a PEM fuel cell is developed. This model couples the flow, species, electrical potential and current density distributions in the two flow channels, two gas diffusion layers, two catalyst layers, and the membrane, respectively. In the flow channel and gas diffuser, a two-phase flow and multi-component model is used. In the cathode catalyst layer, a pseudo-homogeneous model is used. For water transport through the membrane, the model includes the electro-osmotic drag, diffusion and hydraulic permeation. The changes of membrane proton conductivity and dimension with water content in the membrane are also incorporated in the model.

The governing equations on the cathode and anode sides, as well as those for the membrane are coupled in a two-phase flow model, thus they can provide realistic information on various parameter effects. Specifically, water contents in the anode and cathode channels, gas diffusion layers and catalyst layers are coupled by the membrane water transfer; therefore, realistic water distribution in the whole fuel cell sandwich can be obtained. A comparison of the predicated polarization curves with the experimental data showed reasonable agreement.

Acknowledgment

The financial support of the US Department of Energy's CARAT program under contract DE-FC02-98EE50531 is gratefully acknowledged.

References

[1] M.W. Verbrugge, R.F. Hill, Ion and solvent transport in ion-exchange membranes, J. Electrochem. Soc. 137 (1990) 886.
[2] M.W. Verbrugge, R.F. Hill, Analysis of promising perfluorosulfonic acid membranes for fuel-cell electrolytes, J. Electrochem. Soc. 137 (1990) 3770.
[3] D.M. Bernardi, M.W. Verbrugge, Mathematical model of a gas diffusion electrode bonded to a polymer electrolyte, AIChE J. 37 (1991) 1151.
[4] D.M. Bernardi, M.W. Verbrugge, A mathematical model for the solid-polymer-electrode fuel cell, J. Electrochem. Soc. 139 (1992) 2477.
[5] F.E. Springer, T.A. Zawodzinski, S. Gottesfeld, Polymer electrolyte fuel cell model, J. Electrochem. Soc. 138 (1991) 2334.
[6] T.F. Fuller, J. Newman, Water and thermal management in solid-polymer-electrolyte fuel cells, J. Electrochem. Soc. 5 (1993) 1218.
[7] T.V. Nguyen, R.E. White, A water and thermal management model for proton-exchange-membrane fuel cells, J. Electrochem. Soc. 40 (1993) 2178.
[8] V. Gurau, H.T. Liu, S. Kakac, Two-dimensional model for proton exchange membrane fuel cells, AIChE J. 44 (1998) 2410.
[9] C.Y. Wang, Fundamental models for fuel cell engineering, Chem. Rev. 104 (2004) 4727–4765.
[10] A.Z. Weber, J. Newman, Modeling transport in polymer-electrolyte fuel cells, Chem. Rev. 104 (2004) 4679–4726.
[11] Z.H. Wang, C.Y. Wang, K.S. Chen, Two-phase flow and transport in the air cathode of PEM fuel cells, J. Power Sources 94 (2001) 40–50.
[12] L. You, H.T. Liu, A two-phase flow and transport model for the air cathode in PEM fuel cells, Int. J. Heat Mass Transfer 45 (2002) 2277–2287.
[13] L. You, H.T. Liu, "A two-phase and multicomponent model for the cathode of PEM fuel cells," ASME Congress and Exhibition, New York, 2001.
[14] S. Mazumder, V. Cole, Rigorous 3-D mathematical modeling of PEM fuel cells, J. Electrochem. Soc. 150 (2003) A1510–A1517.
[15] T. Berning, N. Djilali, A 3D, multiphase, multicomponent model of the cathode and anode of a PEM fuel cell, J. Electrochem. Soc. 150 (2003) A1589–A1598.
[16] J. Nam, M. Kaviany, Effective diffusivity and water-saturation distribution in single- and two-layer PEMFC diffusion medium, Int. J. Heat Mass Transfer 46 (2003) 4595–4611.
[17] U. Pasaogullari, C.Y. Wang, Liquid water transport in gas diffusion layer of polymer electrolyte fuel cells, Electrochem. Soc. 151 (2004) A399–A406.
[18] L. You, H.T. Liu, A parametric study of the cathode catalyst layer of PEM fuel cells using a pseudo-homogeneous model, Int. J. Hydrogen Energy 25 (2001) 991–999.
[19] C.Y. Wang, P. Cheng, A multiphase mixture model for multiphase, multi-component transport in capillary porous media. I. Model development, Int. J. Heat Mass Transfer 39 (1996) 3607.
[20] K. Vafai, C.L. Tien, Boundary and inertia effects on flow and heat transfer in porous media, Int. J. Heat Mass Transfer 24 (1981) 195.
[21] K.R. Weisbrod, S.A. Grot, N. Vanderborgh, Through-the-electrode model of a proton exchange membrane fuel cell, in: S. Gottesfeld (Ed.), Proceedings of 1st International Symposium on Proton Conducting Membrane Fuel Cells, vol. 152, The Electrochemical Society, New Jersey, 1995, pp. 23–95.
[22] M. Eikerling, A.A. Kornyshev, Modeling the performance of the cathode catalyst layer of polymer electrolyte fuel cells, J. Electroanal. Chem. 453 (1998) 89.
[23] J.S. Newman, Electrochemical Systems, Prentice-Hall, New Jersey, 1991.

[24] J.S. Yi, T.V. Nguyen, An along-the-channel model for PEM fuel cells, J. Electrochem. Soc. 145 (1998) 1149.
[25] J.S. Yi, T.V. Nguyen, Multicomponent transport in porous electrodes of PEM fuel cells using the interdigitated gas distributors, J. Electrochem. Soc. 146 (1999) 38.
[26] A.J. Bard, L.R. Faulkner, Electrochemical Methods: Fundamentals and Applications, John Wiley and Sons, New York, 1980.
[27] Z. Huang, Experimental and Mathematical Studies of PEM Fuel Cell Performances, University of Miami, M.S. Thesis, 2000.